

Cavity-Free Optical Isolators and Circulators Using a Chiral Cross-Kerr Nonlinearity

Keyu Xia,^{1,2,3,*} Franco Nori,^{3,4} and Min Xiao^{1,2,5}

¹National Laboratory of Solid State Microstructures, College of Engineering and Applied Sciences, and School of Physics, Nanjing University, Nanjing 210093, China

²Collaborative Innovation Center of Advanced Microstructures, Nanjing University, Nanjing 210093, China

³Theoretical Quantum Physics Laboratory, RIKEN Cluster for Pioneering Research, Wako-shi, Saitama 351-0198, Japan

⁴Physics Department, The University of Michigan, Ann Arbor, Michigan 48109-1040, USA

⁵Department of Physics, University of Arkansas, Fayetteville, Arkansas 72701, USA



(Received 23 August 2018; published 14 November 2018)

Optical nonlinearity has been widely used to try to produce optical isolators. However, this is very difficult to achieve due to dynamical reciprocity. Here, we show the use of the chiral cross-Kerr nonlinearity of atoms at room temperature to realize optical isolation, circumventing dynamical reciprocity. In our approach, the chiral cross-Kerr nonlinearity is induced by the thermal motion of N -type atoms. The resulting cross phase shift and absorption of a weak probe field are dependent on its propagation direction. This proposed optical isolator can achieve more than 30 dB of isolation ratio, with a low loss of less than 1 dB. By inserting this atomic medium in a Mach-Zehnder interferometer, we further propose a four-port optical circulator with a fidelity larger than 0.9 and an average insertion loss less than 1.6 dB. Using atomic vapor embedded in an on-chip waveguide, our method may provide chip-compatible optical isolation at the single-photon level of a probe field.

DOI: 10.1103/PhysRevLett.121.203602

Introduction.—Optical isolation is highly desirable for lasers, optical information processing, and quantum networks [1,2]. It requires optical nonreciprocity, i.e., breaking of Lorentz reciprocity [3], but is very challenging to achieve without applying magnetic fields.

Nonmagnetic optical isolation is chip compatible and therefore is in great demand for integrated optical signal processing. It has been studied via dynamically modulating material permittivity [4–7], inducing a photonic Berry phase [8–11], twisting a resonator [12], a fast spinning resonator [13], or using optomechanical systems [10, 14–16]. Over the past decades, optical nonlinearity (in particular, Kerr or Kerr-like nonlinearity) has attracted intense research as a chip-compatible candidate for magnetic-free optical isolation [17–22]. Moreover, using a gain medium has also been demonstrated for optical isolation [19–21,23,24]. However, optical isolators with nonlinearity or gain in the medium are subject to dynamic reciprocity [25,26]. Therefore, this kind of device is nonreciprocal only for strong signals with particular intensity but fails to isolate weak signals. A chiral gain has been recently used to overcome this fundamental barrier in nonlinear isolators [22,23]. However, a passive nonlinear isolator without dynamic reciprocity would be of interest. Moreover, most of the existing schemes for optical isolation require high-quality resonators or cryogenic temperatures.

Instead of classical optics, quantum optics provides a tool to control photon propagation, including electromagnetically induced transparency (EIT) [27–29], optical

nonreciprocity [30–32], and chirality [33–38]. Light propagating in a “moving” Bragg lattice created in atoms is subject to a “macroscopic” Doppler effect and has demonstrated nonreciprocity [39–41]. By using a chiral quantum system, optical isolation has been achieved at the single-photon level [42–45].

Optical chirality has been widely exploited to engineer spin-orbital interaction of light [33–37]. In this Letter, we propose how to achieve efficient optical isolation using chiral cross-Kerr (XKerr) nonlinearity induced in atoms. Because of the chirality of atomic nonlinearity, the phases and amplitudes of the forward- (right-) and backward-moving (left-moving) probe fields are very different after passing through atoms along two opposite directions. Therefore, both an optical isolator and a circulator can be achieved with a high isolation ratio and low insertion loss. Because the induced nonlinearity is chiral, our proposals circumvent the problem of dynamic reciprocity and may provide a new cavity-free route for nonlinear optical isolators and circulators.

System and model.—Our setup is depicted in Fig. 1. We first consider a waveguide (WG) embedded with N -type atoms [46–50]; see the upper waveguide in Fig. 1(a). We apply the classical switching and coupling fields to induce the phase shift ϕ and amplitude modulation ξ of the probe field. To a good approximation, we treat the waveguide as a 1D space. If the forward and backward amplitude transmissions ξ_f and ξ_b are sufficiently different after the probe field passes through the ensemble of atoms, then we can

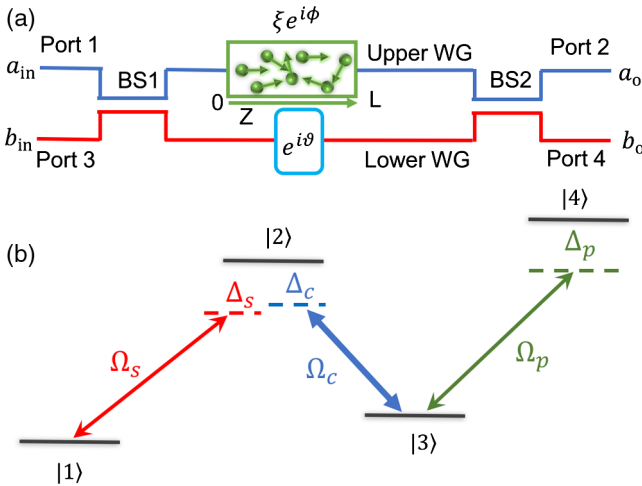


FIG. 1. (a) Schematic diagram of our setup for an optical isolator and circulator. For an optical isolator, we consider only the upper channel embedded with a cloud of N -type atoms. The photon passing through the atoms suffers a phase shift ϕ and an amplitude transmission of ξ , dependent on its propagation direction. To perform an optical circulator, the lower channel is added to form a Mach-Zehnder interferometer, using beam splitters BS1 and BS2, with the upper one. In the lower branch, a phase shift ϑ is used to compensate the phase shift of the backward-moving photon in the upper branch. (b) Level diagram of N -type atoms. The switching (Ω_s), coupling (Ω_c), and probe (Ω_p) fields couple to the transitions $|1\rangle \leftrightarrow |2\rangle$, $|3\rangle \leftrightarrow |2\rangle$, and $|3\rangle \leftrightarrow |4\rangle$, with detunings Δ_s , Δ_c , and Δ_p , respectively.

realize a two-port optical isolator. By carefully choosing the density and length of the atomic vapor and properly arranging the switching and coupling fields, we can obtain a phase shift difference, $\Delta\phi = \phi_f - \phi_b$, approaching π with high transmissions ξ_f and ξ_b . This can provide a four-port optical circulator by adding a lower waveguide to form a Mach-Zehnder interferometer (MZI).

We consider an N -type configuration using rubidium (Rb) atoms to create the chiral XKerr nonlinearity. State $|2\rangle$ decays to states $|1\rangle$ and $|3\rangle$ with rates γ_{21} and γ_{23} , respectively. State $|4\rangle$ decays at a rate γ_{43} . The dephasing rates of both ground states $|1\rangle$ and $|3\rangle$ are Γ . For simplicity, we assume $\gamma_{21} = \gamma_{23} = \gamma_{34} = \gamma_0$ and $\Gamma \ll \gamma_0$, and set $\gamma_0 = 2\pi \times 6$ MHz [51]. The XKerr nonlinearity can be efficiently induced between the probe and switching fields in the configuration shown in Fig. 1(b) and can be modified by the coupling laser [52]. The switching, coupling, and probe laser beams have carrier frequencies ω_s , ω_c , and ω_p , corresponding to wave vectors k_s , k_c , and k_p , respectively. The switching (coupling, probe) field drives the transition $|1\rangle \leftrightarrow |2\rangle$ ($|3\rangle \leftrightarrow |2\rangle$, $|3\rangle \leftrightarrow |4\rangle$) with a detuning Δ_s (Δ_c , Δ_p) in the absence of thermal motion. At room temperature, the inevitable random thermal motion of the j th atom moving with velocity v_j causes the “microscopic” Doppler shifts $k_s v_j$, $k_c v_j$, and $k_p v_j$ in the corresponding atomic transitions, respectively. The strength of the

nonlinearity is strongly dependent on the effective detunings and thus the Doppler shifts. Thus, these frequency shifts change the optical nonlinearity in a way strongly dependent on the propagation direction of the probe field with respect to the switching and coupling fields, leading to the chiral XKerr nonlinearity. We assume that $|k_s| = |k_c| = |k_p| = k$. Both the switching and coupling laser beams are left moving such that $k_s v_j = k_c v_j$. In the above arrangement, the backward-moving (forward-moving) probe field “sees” the same (opposite) Doppler shift as the switching and coupling ones. Under the two-photon resonance condition, i.e., $\Delta_c = \Delta_s = \delta$, and $|\Omega_s| \ll |\Omega_c|$ leading to $\rho_{11} \approx 1$, we can solve the master equation with the perturbation approach [53–55] and obtain the total XKerr nonlinearity averaged over the velocity distribution as [56–60]

$$\chi_f = X_0 \int \frac{\gamma_{23}}{(i\Delta_p + \gamma_{43})} \left(\frac{1}{\zeta} + \frac{1}{\zeta^*} \right) N(v) dv \quad (1)$$

for the forward-moving probe field and

$$\chi_b = X_0 \int \frac{\gamma_{23}}{[i(\Delta_p + 2kv) + \gamma_{43}]} \left(\frac{1}{\zeta} + \frac{1}{\zeta^*} \right) N(v) dv \quad (2)$$

in the backward-moving case, where $X_0 = 3\pi c^2 \gamma_{43} / 8\omega_p^2 \Gamma_3 (\gamma_{21} + \gamma_{23})$, $\zeta = i(\delta + kv) + (\gamma_{21} + \gamma_{23} + \Gamma_3) + |\Omega_c|^2 / 2\Gamma_3$, and c is the vacuum light speed. The velocity distribution is conventionally taken to be Maxwellian, i.e., $N(v) = N_a e^{-v^2/u^2} / \sqrt{\pi u}$, where u is the room-mean-square atomic velocity and $ku \approx 2\pi \times 300$ MHz for Rb atoms at room temperature [61]. In our arrangement, the linear susceptibility of the probe light is vanishingly small and can be neglected because $\rho_{33} \approx 0$. Compared with the backward input case, where the Doppler broadening significantly reduces the total XKerr nonlinearity [see Eq. (2)], the Doppler shift “seen” by the forward-moving probe field is partly compensated [see Eq. (1)], and subsequently the nonlinearity remains large. This chirality is a combination of thermal motion and the unidirectionality of the switching and coupling lasers. The Doppler shift is due to the atomic thermal motion. The unidirectionally propagating switching and coupling lasers break the spatial symmetry, leading to a direction-dependent response to the probe laser. Without the switching and coupling fields, the thermal motion sharply suppresses the atomic susceptibility in both directions. If the control fields in EIT are applied to atoms from two opposite directions, thermal motion will be detrimental [39,40]. In the two latter cases, the chirality disappears. Note that the reduced absorption in the “two-photon Doppler-free” configuration for EIT in a 3D atomic sample has been observed [62]. The two-port nonreciprocal transport has been experimentally demonstrated as a result of atomic thermal motion and the strong atom-cavity coupling [63]. However, cavity-free

optical isolation exploiting thermal motion is conceptually different and admirable, because its realization can be simpler and it can implement multiport optical circulators.

Unlike the configurations for quantum gates [51] and nondestructive detection of photons [64], the applied switching and coupling modes are chosen here to be much stronger than the probe laser beam. The backaction on the switching field due to the probe photon is negligible. Thus, they can be considered as constant in atoms. We apply the slowly varying envelope approximation to the probe field. The backscattering is negligible during the propagation, and the probe photon propagates unidirectionally [51,65]. When $|\Omega_c| \gg |\Omega_s| \gg |\Omega_p|$, the propagation of the probe pulse in atoms is described by Maxwell equations by taking into account the XKerr nonlinearity [66,67]:

$$\frac{\partial \Omega_p^f(z, t)}{\partial z} + \frac{1}{c} \frac{\partial \Omega_p^f(z, t)}{\partial t} = -\chi_f |\Omega_s|^2 \Omega_p^f(z, t), \quad (3)$$

$$\frac{\partial \Omega_p^b(z', t)}{\partial z'} + \frac{1}{c} \frac{\partial \Omega_p^b(z', t)}{\partial t} = -\chi_b |\Omega_s|^2 \Omega_p^b(z', t) \quad (4)$$

for the forward- and backward-moving probe pulses, respectively, and $z' = L - z$. When $\chi_f = \chi_b$ as in the usual Kerr nonlinear isolators, the medium is reciprocal for the probe beam. However, the medium can be nonreciprocal even for two weak counterpropagating probe beams coexisting in the medium simultaneously when χ_f and χ_b are very different. Therefore, optical isolators or circulators using this chiral medium can overcome the dynamical reciprocity in conventional nonlinear isolators [25]. We focus on the steady-state solution, where a long probe pulse is constant in time at position z [51], such that $(1/c)(\partial \Omega_p^f/\partial t) \approx 0$ and $(1/c)(\partial \Omega_p^b/\partial t) \approx 0$. After passing through the atomic medium with length L , the probe fields become

$$\Omega_p^j(L) = \xi_j e^{i\phi_j} \Omega_p^j(0), \quad (5)$$

where $\xi_j = \exp(-\text{Re}[\chi_j]|\Omega_s|^2 L)$ and $\phi_j = -\text{Im}[\chi_j]|\Omega_s|^2 L$, with $j = f, b$, are the corresponding transmission amplitude and phase shift, respectively. When $|\Delta_p| \gg \gamma_{43}$ and $|\Omega_c|^2/2\Gamma_3 \gg |\delta + kv|$, to a good approximation, we have $\phi_f \approx N_a L (3\pi c^2/4\omega_p^2) (\gamma_0/\Delta_p) (|\Omega_s|^2/|\Omega_c|^2)$ and $\xi_f \approx \exp[-N_a L (3\pi c^2/4\omega_p^2) (\gamma_0^2/\Delta_p^2) (|\Omega_s|^2/|\Omega_c|^2)]$. The transmission is calculated as $|\xi_j|^2$. In contrast, the transmission and phase modulation of the backward-moving probe laser are much smaller.

Obviously, an optical isolator can be realized when $\xi_f \gg \xi_b$. For $\xi_f \approx \xi_b$ and $\phi_f - \phi_b \approx \pi$, an optical circulator could be made by inserting the atomic vapor in an MZI, as shown in Fig. 1(a). To achieve that, two beam splitters (BSs) are needed to first divide the input probe pulse into two paths and then mix them after passing through the

nonlinear medium. The two BSs are chosen to be identical with reflection and transmission amplitudes of $\sin \theta$ and $\cos \theta$, respectively. The relative phase in these amplitudes is φ . Their operation on photons is determined by $H_{\text{BS}} = \theta e^{i\varphi} \hat{a}_{\text{in}}^\dagger \hat{b}_{\text{in}} + \theta e^{-i\varphi} \hat{a}_{\text{in}} \hat{b}_{\text{in}}^\dagger$ [68]. A fixed phase shift ϑ in the lower path compensates the phase shift ϕ_b of the backward-moving probe laser beam caused by the nonlinear medium. Therefore, the backward-moving probe photons entering BS1 have the same phase in the upper and lower waveguides. Applying H_{BS} and the transmission relation Eq. (5), we obtain the forward transmission matrix elements between the input and output ports as

$$T_{12} = \left| \frac{a_o}{a_{\text{in}}} \right|^2 = |\xi_f e^{i(\phi_f - \vartheta)} \cos^2 \theta - \sin^2 \theta|^2, \quad (6a)$$

$$T_{32} = \left| \frac{a_o}{b_{\text{in}}} \right|^2 = |(1 + \xi_f e^{i(\phi_f - \vartheta)}) \cos \theta \sin \theta|^2, \quad (6b)$$

$$T_{14} = \left| \frac{b_o}{a_{\text{in}}} \right|^2 = |(1 + \xi_f e^{i(\phi_f - \vartheta)}) \cos \theta \sin \theta|^2, \quad (6c)$$

$$T_{34} = \left| \frac{b_o}{b_{\text{in}}} \right|^2 = |\cos^2 \theta - \xi_f e^{i(\phi_f - \vartheta)} \sin^2 \theta|^2, \quad (6d)$$

where T_{mn} is the transmission coefficient from port m to port n , with $m, n = 1, 2, 3, 4$. Exchanging the inputs and the outputs and replacing ξ_f and ϕ_f with ξ_b and ϕ_b in T_{mn} , respectively, we obtain the transmission matrix element T_{nm} for the backward-moving case. Optical nonreciprocity requires $T_{mn} \neq T_{nm}$ for $m \neq n$. We have $T_{mm} = 0$ in the circulator. Also, the backscattering to ports at the same side as the input is negligible so that $T_{31} = T_{13} = T_{41} = T_{14}$ (see details in Supplemental Material [56]). An ideal circulator, in which the photons flow along $1 \rightarrow 2 \rightarrow 3 \rightarrow 4 \rightarrow 1$, has a transmission matrix T^{id} with elements $T_{12}^{\text{id}} = T_{23}^{\text{id}} = T_{34}^{\text{id}} = T_{41}^{\text{id}} = 1$ and others zero. Note that $\text{Tr}[T^{\text{id}} T^{\text{id},T}] = 4$.

Hereafter, we take $\delta = 0$ and $\omega_p/2\pi \sim 384$ THz for the D_1 line of Rb atoms and choose the parameters $N_a = 5 \times 10^{12} \text{ cm}^{-3}$, $\Gamma_3 = 0.1\gamma_0$, $\Omega_c = 20\gamma_0$, and $\Omega_s = 4\gamma_0$, yielding $\rho_{11} \approx 0.96$. Such large switching light can enhance the cross phase modulation of the probe field.

Isolator.—For a centimeter-scale medium, e.g., $L = 2$ cm, the medium is absorptive. The forward and backward transmissions are very different; see Fig. 2. As the probe detuning increases, the forward transmission T_{12} rapidly increases to a high value of 0.80 at $\Delta_p = 35.6\gamma_0$, corresponding to an insertion loss of 1 dB. Because of Doppler broadening, the backward-moving probe field suffers a larger absorption. Therefore, the backward transmission T_{21} is much smaller than T_{12} , when $35.6\gamma_0 < \Delta_p < 60.6\gamma_0$. In this region, the insertion loss is smaller than 1 dB, while the isolation ratio is larger than 15 dB. The isolation ratio

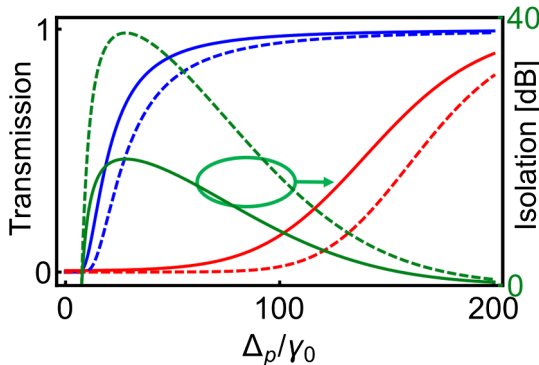


FIG. 2. Transmission of an isolator for the right-moving (blue curves) and left-moving (red curves) probe fields and the isolation ratio (green curves associating with the right vertical axis) as a function of the probe detuning Δ_p . Solid (dashed) curves are for $L = 2(4)$ cm. Other parameters are $N_a = 5 \times 10^{12} \text{ cm}^{-3}$, $\Gamma_3 = 0.1\gamma_0$, $\Omega_c = 20\gamma_0$, $\Omega_s = 4\gamma_0$, and $\delta = 0$.

can be considerably improved with a large forward transmission by using a longer medium or, equivalently, increasing the atomic density. The nonreciprocal window of frequency slightly moves to larger detuning. For $L = 4$ cm, the isolation ratio can reach more than 30 dB in the range of $50\gamma_0 < \Delta_p < 60\gamma_0$, yielding an isolation bandwidth of $2\pi \times 60$ MHz. At the same time, the insertion loss remains low, less than 1 dB. Thus, we can simply use this medium as an isolator.

Circulator.—For a short medium, the transmissions of the forward- and backward-moving probes can be comparably high. However, at a particular probe frequency, the phase shift difference between these two opposite propagating probes can approach π . As shown in Fig. 3(a), for $L = 3.33$ mm, the phase shift ϕ_b is always small, specifically about 0.011π at $\Delta_p = 7.77\gamma_0$. In contrast, ϕ_f exponentially decays from about 2π at $\Delta_p = 3.5\gamma_0$ to 0.5π at $\Delta_p = 15.5\gamma_0$. At the optimal point $\Delta_p^{\text{opt}} = 7.77\gamma_0$, the difference of phase shifts, $\phi_f - \phi_b$, reaches the optimal value of π . At this point, $\xi_f^{\text{opt}} \approx \xi_b^{\text{opt}} \approx 0.66$. Thus, a high-performance circulator can be made by inserting this nonlinear medium into an MZI composed of unbalanced BSs. Here, we set $\vartheta = 0.01\pi$ and $\sin^2 \theta = 0.4 \approx \bar{\xi}/(1 + \bar{\xi})$ with $\bar{\xi} = (\xi_f^{\text{opt}} + \xi_b^{\text{opt}})/2$.

The performance of a circulator can be quantified with the fidelity \mathcal{F} and the average photon survival probability η [43]. The fidelity is evaluated as the overlap of the renormalized transmission matrix $\tilde{T} = (T_{ij}/\eta_i)$ with the ideal one, T^{id} . Here, $\eta_i = \sum_k T_{i,k}$ is the survival probability of the probe photons entering port i . The average operation fidelity of the circulator is then $\mathcal{F} = \text{Tr}[\tilde{T}T^{\text{id},T}]/\text{Tr}[T^{\text{id}}T^{\text{id},T}]$, giving the probability of a correct circulator operation averaged over various inputs. The minimum fidelity is $\mathcal{F} = 0$, while an ideal operation yields $\mathcal{F} = 1$. The average photon survival probability $\eta = \sum_i \eta_i/4$ is

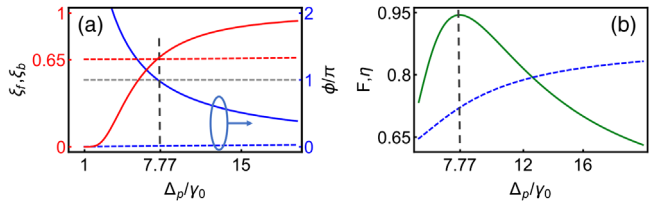


FIG. 3. Circulator performance versus the detuning Δ_p . (a) Phase shifts (blue curves) and transmission amplitudes (red curves) for right- (solid curves) and left-moving (dashed lines) probe fields as a function of the probe detuning Δ_p . (b) Fidelity (green curves) and average insertion loss (blue dashed curves) of an optical circulator as a function of Δ_p . The vertical black dashed lines in the two figures show the optimal detuning $\Delta_p^{\text{opt}}/\gamma_0 = 7.77$ when $\phi_f^{\text{opt}} - \phi_b^{\text{opt}} = \pi$ and $\xi_f^{\text{opt}} \approx \xi_b^{\text{opt}} \approx 0.66$. The length of the atomic medium is 3.33 mm. Other parameters are as in Fig. 2.

another important figure characterizing the four-port circulator. We scan the probe frequency to find the working window of the circulator in Fig. 3. As the detuning Δ_p varies from $6\gamma_0$ to $20\gamma_0$, the fidelity first rises up rapidly, reaches the maximum 0.944 at $\Delta_p^{\text{opt}} = 7.77\gamma_0$, and then decreases to a small value of 0.63. During this sweep, η increases from 0.68 to about 0.83. Although the photons have a larger probability to survive at a large detuning, the fidelity is low. As a trade-off, the circulator operating within the frequency range $6.6\gamma_0 < \Delta_p < 9.7\gamma_0$ can achieve a fidelity larger than 0.9 at the expense of $\eta > 0.69$. The corresponding working window is about $2\pi \times 20$ MHz, and the average insertion loss is about 1.6 dB. If $\vartheta = 0$, the fidelity and insertion loss reduce only very slightly.

At Δ_p^{opt} , we obtain $\mathcal{F} = 0.944$ and $\eta = 0.72$, yielding an insertion loss of 1.42 dB. The corresponding transmission matrix is shown in Fig. 4. The obtained matrix is close to that of the ideal circulator, implying that a good optical nonreciprocity is obtained. We can also quantify the circulator performance by the isolations $I_i = -10 \log(T_{i+1,i}/T_{i,i+1})$ of the four optical isolators formed between adjacent ports [43] and have $\{I_i\} = \{41.7, 13.8, 13.8, 8.2\}$ dB with $i = \{1, 2, 3, 4\}$, implying nonreciprocal photon circulation along $1 \rightarrow 2 \rightarrow 3 \rightarrow 4 \rightarrow 1$. The achieved performance is already useful for practical optical isolation [43].

Implementation.—The required 1D nonlinear waveguide embedded with alkali atoms can be made with various methods and platforms [42,46–50,69–74]. A feasible platform can be a centimeter-scale hollow-core photonic crystal fiber filled with Rb atoms at room temperature [49,74]. A few-photon-level memory and a strong XKerr nonlinearity have been demonstrated with a weak control field in such a platform [49,74]. For an on-chip realization, we consider a zigzag waveguide cladded with high-density Rb atoms, allowing a coherent light-atom interaction [71–73]. To conduct an N -type configuration, we couple the lasers

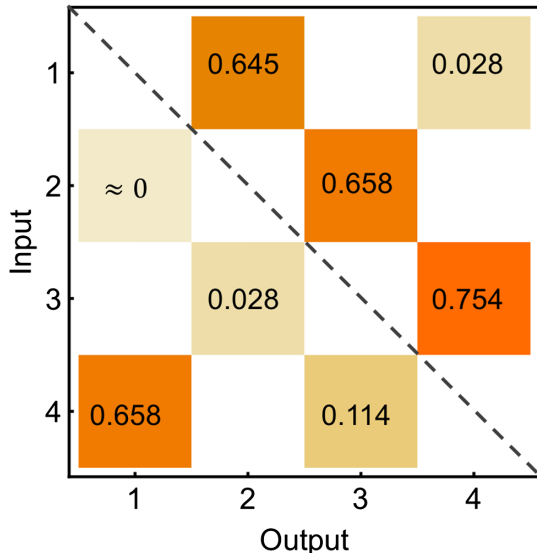


FIG. 4. Transmission matrix of an optical circulator at the optimal point $\Delta_p^{\text{opt}}/\gamma_0 = 7.77$. The numbers inside the color squares are the transmission between the two ports. The transmissions in white areas are zero. Other parameters are as in Fig. 3.

to the D_1 lines of the Rb atom, yielding $\omega_p/2\pi \sim 384$ THz. A linearly polarized probe field drives the transition $|5^2S_{1/2}, F=2, m_s=0\rangle \leftrightarrow |5^2P_{1/2}, F'=2, m'_s=0\rangle$. The linearly polarized switching light couples to $|5^2S_{1/2}, F=1, m_s=-1\rangle \leftrightarrow |5^2P_{1/2}, F'=1, m'_s=-1\rangle$. The strong left-circularly-polarized coupling field is applied between $|5^2S_{1/2}, F=2, m_s=0\rangle \leftrightarrow |5^2P_{1/2}, F'=1, m'_s=-1\rangle$. Thus, the optical isolation can be performed for a linearly polarized light.

Conclusion.—We have presented new ways to realize optical isolators and circulators using chiral XKerr nonlinearity of N -type atoms embedded in a 1D waveguide. The four-port optical circulator can reach a high fidelity of 0.9 and a small insertion loss of 1.6 dB. Our proposal may provide a new vision for nonlinear optical isolation without dynamic reciprocity, because the XKerr nonlinearity itself is chiral, and the isolation is based on the linear Eqs. (3) and (4). A large XKerr nonlinearity has been reported at the single-photon level [49,51]. Therefore, our method can be extended to the quantum regime, realizing an optical circulator for a single-photon probe on a chip at room temperature.

We acknowledge Dr. Sahin Ozdemir for helpful discussions. K. X. and M. X. thank the support of the National Key R&D Program of China (Grant No. 2017YFA0303703) and the National Natural Science Foundation of China (Grants No. 11874212 and No. 61435007). F. N. is supported in part by the MURI Center for Dynamic Magneto-Optics via the Air Force Office of Scientific Research (AFOSR) (FA9550-14-1-0040), Army Research Office (ARO) (Grant No. W911NF-18-1-0358), Asian Office of Aerospace

Research and Development (AOARD) (Grant No. FA2386-18-1-4045), Japan Science and Technology Agency (JST) (the ImPACT program and CREST Grant No. JPMJCR1676), Japan Society for the Promotion of Science (JSPS) (JSPS-RFBR Grant No. 17-52-50023 and JSPS-FWO Grant No. VS.059.18N), RIKEN-AIST Challenge Research Fund, and the John Templeton Foundation.

*keyu.xia@nju.edu.cn

- [1] J. I. Cirac, P. Zoller, H. J. Kimble, and H. Mabuchi, Quantum State Transfer and Entanglement Distribution among Distant Nodes in a Quantum Network, *Phys. Rev. Lett.* **78**, 3221 (1997).
- [2] H. J. Kimble, The quantum internet, *Nature (London)* **453**, 1023 (2008).
- [3] D. Jalas, A. Petrov, M. Eich, W. Freude, S. Fan, Z. Yu, R. Baets, M. Popović, A. Melloni, J. D. Joannopoulos, M. Vanwolleghem, C. R. Doerr, and H. Renner, What is—and what is not—an optical isolator, *Nat. Photonics* **7**, 579 (2013).
- [4] Z. Yu and S. Fan, Optical isolation based on nonreciprocal phase shift induced by interband photonic transitions, *Appl. Phys. Lett.* **94**, 171116 (2009).
- [5] D. L. Sounas and A. Alù, Non-reciprocal photonics based on time modulation, *Nat. Photonics* **11**, 774 (2017).
- [6] Z. Yu and S. Fan, Complete optical isolation created by indirect interband photonic transitions, *Nat. Photonics* **3**, 91 (2009).
- [7] M. S. Kang, A. Butsch, and P. St. J. Russell, Reconfigurable light-driven opto-acoustic isolators in photonic crystal fibre, *Nat. Photonics* **5**, 549 (2011).
- [8] K. Fang, Z. Yu, and S. Fan, Realizing effective magnetic field for photons by controlling the phase of dynamic modulation, *Nat. Photonics* **6**, 782 (2012).
- [9] K. Fang, Z. Yu, and S. Fan, Photonic Aharonov-Bohm Effect Based on Dynamic Modulation, *Phys. Rev. Lett.* **108**, 153901 (2012).
- [10] K. Fang, J. Luo, A. Metelmann, M. H. Matheny, F. Marquardt, A. A. Clerk, and O. Painter, Generalized nonreciprocity in an optomechanical circuit via synthetic magnetism and reservoir engineering, *Nat. Phys.* **13**, 465 (2017).
- [11] L. D. Tzoung, K. Fang, P. Nussenzveig, S. Fan, and M. Lipson, Non-reciprocal phase shift induced by an effective magnetic flux for light, *Nat. Photonics* **8**, 701 (2014).
- [12] N. Jia, N. Schine, A. Georgakopoulos, A. Ryou, A. Sommer, and J. Simon, Photons and polaritons in a broken-time-reversal nonplanar resonator, *Phys. Rev. A* **97**, 013802 (2018).
- [13] S. Maayani, R. Dahan, Y. Kligerman, E. Moses, A. U. Hassan, H. Jing, F. Nori, D. N. Christodoulides, and T. Carmon, Flying couplers above spinning resonators generate irreversible refraction, *Nature (London)* **558**, 569 (2018).
- [14] M. Hafezi and P. Rabl, Optomechanically induced nonreciprocity in microring resonators, *Opt. Express* **20**, 7672 (2012).

- [15] Z. Shen, Y.-L. Zhang, Y. Chen, C.-L. Zou, Y.-F. Xiao, X.-B. Zou, F.-W. Sun, G.-C. Guo, and C.-H. Dong, Experimental realization of optomechanically induced non-reciprocity, *Nat. Photonics* **10**, 657 (2016).
- [16] F. Ruesink, M.-A. Miri, A. Alù, and E. Verhagen, Nonreciprocity and magnetic-free isolation based on optomechanical interactions, *Nat. Commun.* **7**, 13662 (2016).
- [17] M. Soljačić, C. Luo, J. D. Joannopoulos, and S. Fan, Nonlinear photonic crystal microdevices for optical integration, *Opt. Lett.* **28**, 637 (2003).
- [18] L. Fan, J. Wang, L. T. Varghese, H. Shen, B. Niu, Y. Xuan, A. M. Weiner, and M. Qi, An all-silicon passive optical diode, *Science* **335**, 447 (2012).
- [19] L. Chang, X. Jiang, S. Hua, C. Yang, J. Wen, L. Jiang, G. Li, G. Wang, and M. Xiao, Parity-time symmetry and variable optical isolation in active-passive-coupled microresonators, *Nat. Photonics* **8**, 524 (2014).
- [20] B. Peng, Ş. K. Özdemir, F. Lei, F. Monifi, M. Gianfreda, G. L. Long, S. Fan, F. Nori, C. M. Bender, and L. Yang, Parity-time-symmetric whispering-gallery microcavities, *Nat. Phys.* **10**, 394 (2014).
- [21] N. Bender, S. Factor, J. D. Bodyfelt, H. Ramezani, D. N. Christodoulides, F. M. Ellis, and T. Kottos, Observation of Asymmetric Transport in Structures with Active Nonlinearities, *Phys. Rev. Lett.* **110**, 234101 (2013).
- [22] S. Hua, J. Wen, X. Jiang, Q. Hua, L. Jiang, and M. Xiao, Demonstration of a chip-based optical isolator with parametric amplification, *Nat. Commun.* **7**, 13657 (2016).
- [23] Y. Zheng, J. Yang, Z. Shen, J. Cao, X. Chen, X. Liang, and W. Wan, Optically induced transparency in a micro-cavity, *Light Sci. Appl.* **5**, e16072 (2016).
- [24] B. He, L. Yang, X. Jiang, and M. Xiao, Transmission Nonreciprocity in a Mutually Coupled Circulating Structure, *Phys. Rev. Lett.* **120**, 203904 (2018).
- [25] Y. Shi, Z. Yu, and S. Fan, Limitations of nonlinear optical isolators due to dynamic reciprocity, *Nat. Photonics* **9**, 388 (2015).
- [26] A. B. Khanikaev and A. Alù, Nonlinear dynamic reciprocity, *Nat. Photonics* **9**, 359 (2015).
- [27] B. Peng, Ş. K. Özdemir, W. Chen, F. Nori, and L. Yang, What is and what is not electromagnetically induced transparency in whispering-gallery microcavities, *Nat. Commun.* **5**, 5082 (2014).
- [28] H.-C. Sun, Y.-x. Liu, H. Ian, J. Q. You, E. Il'ichev, and F. Nori, Electromagnetically induced transparency and Autler-Townes splitting in superconducting flux quantum circuits, *Phys. Rev. A* **89**, 063822 (2014).
- [29] H. Ian, Y.-x. Liu, and F. Nori, Tunable electromagnetically induced transparency and absorption with dressed superconducting qubits, *Phys. Rev. A* **81**, 063823 (2010).
- [30] P. Lodahl, S. Mahmoodian, S. Stobbe, A. Rauschenbeutel, P. Schneeweiss, J. Volz, H. Pichler, and P. Zoller, Chiral quantum optics, *Nature (London)* **541**, 473 (2017).
- [31] C. Y. Hu, Spin-based single-photon transistor, dynamic random access memory, diodes, and routers in semiconductors, *Phys. Rev. B* **94**, 245307 (2016).
- [32] R. Huang, A. Miranowicz, J.-Q. Liao, F. Nori, and H. Jing, Nonreciprocal Photon Blockade, *Phys. Rev. Lett.* **121**, 153601 (2018).
- [33] Y. Tang and A. E. Cohen, Optical Chirality and Its Interaction with Matter, *Phys. Rev. Lett.* **104**, 163901 (2010).
- [34] K. Y. Bliokh, D. Smirnova, and F. Nori, Quantum spin Hall effect of light, *Science* **348**, 1448 (2015).
- [35] K. Y. Bliokh, F. J. Rodríguez-Fortuño, F. Nori, and A. V. Zayats, Spin-orbit interactions of light, *Nat. Photonics* **9**, 796 (2015).
- [36] K. Y. Bliokh and F. Nori, Transverse and longitudinal angular momenta of light, *Phys. Rep.* **592**, 1 (2015).
- [37] K. Y. Bliokh and F. Nori, Characterizing optical chirality, *Phys. Rev. A* **83**, 021803(R) (2011).
- [38] T. Li, A. Miranowicz, X. Hu, K. Xia, and F. Nori, Quantum memory and gates using a Λ -type quantum emitter coupled to a chiral waveguide, *Phys. Rev. A* **97**, 062318 (2018).
- [39] D.-W. Wang, H.-T. Zhou, M.-J. Guo, J.-X. Zhang, J. Evers, and S.-Y. Zhu, Optical Diode Made from a Moving Photonic Crystal, *Phys. Rev. Lett.* **110**, 093901 (2013).
- [40] S. A. R. Horsley, J.-H. Wu, M. Artoni, and G. C. La Rocca, Optical Nonreciprocity of Cold Atom Bragg Mirrors in Motion, *Phys. Rev. Lett.* **110**, 223602 (2013).
- [41] H. Ramezani, P. K. Jha, Y. Wang, and X. Zhang, Nonreciprocal Localization of Photons, *Phys. Rev. Lett.* **120**, 043901 (2018).
- [42] C. Sayrin, C. Junge, R. Mitsch, B. Albrecht, D. O'Shea, P. Schneeweiss, J. Volz, and A. Rauschenbeutel, Nanophotonic Optical Isolator Controlled by the Internal State of Cold Atoms, *Phys. Rev. X* **5**, 041036 (2015).
- [43] M. Scheucher, A. Hilico, E. Will, J. Volz, and A. Rauschenbeutel, Quantum optical circulator controlled by a single chirally coupled atom, *Science* **354**, 1577 (2016).
- [44] I. Söllner, S. Mahmoodian, S. L. Hansen, L. Midolo, A. Javadi, G. Kiršanskė, T. Pregnolato, H. El-Ella, E. H. Lee, J. D. Song, S. Stobbe, and P. Lodahl, Deterministic photon-emitter coupling in chiral photonic circuits, *Nat. Nanotechnol.* **10**, 775 (2015).
- [45] K. Xia, G. Lu, G. Lin, Y. Cheng, Y. Niu, S. Gong, and J. Twamley, Reversible nonmagnetic single-photon isolation using unbalanced quantum coupling, *Phys. Rev. A* **90**, 043802 (2014).
- [46] H. Schmidt and A. R. Hawkins, Electromagnetically induced transparency in alkali atoms integrated on a semiconductor chip, *Appl. Phys. Lett.* **86**, 032106 (2005).
- [47] E. J. Lunt, B. Wu, J. M. Keeley, P. Measor, H. Schmidt, and A. R. Hawkins, Hollow ARROW waveguides on self-aligned pedestals for improved geometry and transmission, *IEEE Photonics Technol. Lett.* **22**, 1147 (2010).
- [48] L. Stern, B. Desiatov, I. Goykhman, and U. Levy, Nanoscale light-matter interactions in atomic cladding waveguides, *Nat. Commun.* **4**, 1548 (2013).
- [49] V. Venkataraman, K. Saha, and A. L. Gaeta, Phase modulation at the few-photon level for weak-nonlinearity-based quantum computing, *Nat. Photonics* **7**, 138 (2013).
- [50] G. Epple, K. S. Kleinbach, T. G. Euser, N. Y. Joly, T. Pfau, P. St. J. Russell, and R. Löw, Rydberg atoms in hollow-core photonic crystal fibres, *Nat. Commun.* **5**, 4132 (2014).
- [51] Z.-Y. Liu, Y.-H. Chen, Y.-C. Chen, H.-Y. Lo, P.-J. Tsai, I. A. Yu, Y.-C. Chen, and Y.-F. Chen, Large Cross-Phase Modulation at the Few-Photon Level, *Phys. Rev. Lett.* **117**, 203601 (2016).

- [52] H. Schmidt and A. Imamoğlu, Giant Kerr nonlinearities obtained by electromagnetically induced transparency, *Opt. Lett.* **21**, 1936 (1996).
- [53] R. W. Boyd, *Nonlinear Optics*, 3rd ed. (Elsevier, New York, 2008).
- [54] Y. Q. Li and M. Xiao, Electromagnetically induced transparency in a three-level Λ -type system in rubidium atoms, *Phys. Rev. A* **51**, R2703 (1995).
- [55] J. Sheng, X. Yang, H. Wu, and M. Xiao, Modified self-Kerr nonlinearity in a four-level N-type atomic system, *Phys. Rev. A* **84**, 053820 (2011).
- [56] See Supplemental Material at <http://link.aps.org/supplemental/10.1103/PhysRevLett.121.203602> for the derivation of the cross-Kerr nonlinearity, which includes Refs. [57–60].
- [57] K. Xia, M. Alamri, and M. S. Zubairy, Ultrabroadband nonreciprocal transverse energy flow of light in linear passive photonic circuits, *Opt. Express* **21**, 25619 (2013).
- [58] K. Okamoto, *Fundamental of Optics Waveguides*, 2nd ed. (Elsevier, New York, 2006).
- [59] H. Wang, D. J. Goorskey, and M. Xiao, Atomic coherence induced Kerr nonlinearity enhancement in Rb vapour, *J. Mod. Opt.* **49**, 335 (2002).
- [60] M. O. Scully and M. Suhail Zubairy, *Quantum Optics*, (Cambridge University, Cambridge, England, 1997).
- [61] H. Wu, J. Gea-Banacloche, and M. Xiao, Observation of Intracavity Electromagnetically Induced Transparency and Polariton Resonances in a Doppler-Broadened Medium, *Phys. Rev. Lett.* **100**, 173602 (2008).
- [62] J. Gea-Banacloche, Y.-Q. Li, S.-Z. Jin, and M. Xiao, Electromagnetically induced transparency in ladder-type inhomogeneously broadened media: Theory and experiment, *Phys. Rev. A* **51**, 576 (1995).
- [63] S. Zhang, Y. Hu, G. Lin, Y. Niu, K. Xia, J. Gong, and S. Gong, Thermal-motion-induced non-reciprocal quantum optical system, *Nat. Photonics*, doi: 10.1038/s41566-018-0269-2 (2018).
- [64] K. Xia, M. Johnsson, P. L. Knight, and J. Twamley, Cavity-Free Scheme for Nondestructive Detection of a Single Optical Photon, *Phys. Rev. Lett.* **116**, 023601 (2016).
- [65] M. Fleischhauer, A. Imamoglu, and J. P. Marangos, Electromagnetically induced transparency: Optics in coherent media, *Rev. Mod. Phys.* **77**, 633 (2005).
- [66] See Supplemental Material at <http://link.aps.org/supplemental/10.1103/PhysRevLett.121.203602> for the propagation equation of the field in a 1D space, which includes Refs. [67].
- [67] K. Xia, S. Q. Gong, C. Liu, X. Song, and Y. Niu, Near dipole-dipole effects on the propagation of few-cycle pulse in a dense two-level medium, *Opt. Express* **13**, 5913 (2005).
- [68] P. Kok, W. J. Munro, K. Nemoto, T. C. Ralph, J. P. Dowling, and G. J. Milburn, Linear optical quantum computing with photonic qubits, *Rev. Mod. Phys.* **79**, 135 (2007).
- [69] F. Le Kien and A. Rauschenbeutel, Electromagnetically induced transparency for guided light in an atomic array outside an optical nanofiber, *Phys. Rev. A* **91**, 053847 (2015).
- [70] T. Nieddu, V. Gokhroo, and S. N. Chormaic, Optical nanofibres and neutral atoms, *J. Opt* **18**, 053001 (2016).
- [71] L. Stern, B. Desiatov, N. Mazurski, and U. Levy, Strong coupling and high-contrast all-optical modulation in atomic cladding waveguides, *Nat. Commun.* **8**, 14461 (2016).
- [72] R. Ritter, N. Gruhler, H. Dobbertin, H. Kübler, S. Scheel, W. Pernice, T. Pfau, and R. Löw, Coupling Thermal Atomic Vapor to Slot Waveguides, *Phys. Rev. X* **8**, 021032 (2018).
- [73] R. Ritter, N. Gruhler, W. Pernice, H. Kübler, T. Pfau, and R. Löw, Atomic vapor spectroscopy in integrated photonic structures, *Appl. Phys. Lett.* **107**, 041101 (2015).
- [74] M. R. Sprague, P. S. Michelberger, T. F. M. Champion, D. G. England, J. Nunn, X.-M. Jin, W. S. Kolthammer, A. Abdolvand, P. St. J. Russell, and I. A. Walmsley, Broadband single-photon-level memory in a hollow-core photonic crystal fibre, *Nat. Photonics* **8**, 287 (2014).